A NODE-BASED SMOOTHED CONFORMING POINT INTERPOLATION METHOD (NS-CPIM) FOR ELASTICITY PROBLEMS

X. XU*

College of Mathematics, Jilin University, 2699 Qianjin Street,

Changchun 130012, P. R. China

School of Engineering System, Queensland University of Technology

GPO Box 2434, Brisbane, QLD4001, Australia

xuxu@jlu.edu.cn

Y. T. Gu

School of Engineering System, Queensland University of Technology

GPO Box 2434, Brisbane, QLD4001, Australia

X. Yang

College of Mathematics, Jilin University, 2699 Qianjin Street,

Changchun 130012, P. R. China

Received 20 August 2010
Revised 23 October 2010

This paper formulates a node-based smoothed conforming point interpolation method (NS-CPIM) for solid mechanics. In the proposed NS-CPIM, the higher order conforming PIM shape functions (CPIM) have been constructed to produce a continuous and piecewise quadratic displacement field over the whole problem domain, whereby the smoothed strain field was obtained through smoothing operation over each smoothing domain associated with domain nodes. The smoothed Galerkin weak form was then developed to create the discretized system equations. Numerical studies have demonstrated the following good properties: NS-CPIM (1) can pass both standard and quadratic patch test; (2) provides an upper bound of strain energy; (3) avoid the volumetric locking; (4) provides the higher accuracy than those in the node-based smoothed schemes of the original PIMs.

Keywords: Meshfree methods; bound solutions, volumetric locking free, patch test.

1. Introduction

Point interpolation method [Gu 2005; Liu and Gu 2001; Liu and Gu (2005); Liu (2009a)] is one of the meshfree methods [Belytschko *et al*. (1994); Liu (1995); Atluri and Zhu

* Corresponding author.

(1998)], which numerical operations such as interpolation and integration are conducted based on nodes. The PIM possesses the following features: (1) shape functions using polynomial basis functions has at least linear terms and ensure that the PIM shape functions possess at least linearly consistency; (2) local supporting nodes selection based on triangular cells can overcome the singular moment matrix issue; (3) the shape functions are of the Delta function property, which facilitates easy implementation of essential boundary conditions; and (4) this set of shape functions are linearly independent and hence forms a basis for displacement field construction [Liu (2009a)].

However, original higher order PIM shape functions are not compatible, and produce discontinuous displacement field when the support domain updated its nodes. In order to obtain a high accuracy solution using PIM, smoothed point interpolation methods (S-PIM) [Liu (2008); Liu (2009b)] that was generalized from the strain smoothing technique [Chen (2001)] are proposed in a framework of weakened weak (W^2) formulation [Liu (2010a), Liu (2010b)]. S-PIM can guarantee the convergence and stability, and have been used in many fields of sciences and engineering.

On the other hand, Xu and Liu *et al*. (2010) proposed a novel conforming point interpolation method (CPIM) for generating higher order PIM shape functions without using the strain smoothing techniques. A technique was developed to install the conformability by reconstructing the shape functions using the original PIM shape functions. A solution with very high accuracy and convergent rate has been obtained using the CPIM [Xu and Liu *et al*. (2010)].

In this paper, by combining the W^2 formulation and CPIM, we develop a node-based smoothing conforming PIM (NS-CPIM). It is the higher order models in the family of the S-PIM models. Intensive numerical examples will be presented to demonstrate the superior effectiveness of the NS-CPIM.

2. CPIM shape functions

In the original PIM, T-schemes are usually used for node selection [Liu and Zhang (2008)]. In the CPIM, problem domain is first discretized by a set of background triangular cells denoted as Ω_i $(i=1,2,...,m)$, and the midpoints of the cell-edge are denoted as q_j $(j=1,2,...,I)$ as shown in Fig. 1.

The overall procedures of shape function construction in the CPIM are as follows: (1) The displacement at any point in a triangular cell is first approximated via the original PIM using T6/3-scheme. This obtained displacement is not continuous along the cell edge between two adjacent cells [Liu (2009a)]. (2) The displacements at the midpoints of cell-edges are assumed to be the simple average of that at midpoints on the interface edge connecting these two adjacent cells:

$$\mathbf{u}\big|_{q_1} = \frac{1}{2}\left[\mathbf{u}(\Omega_1)\big|_{q_1} + \mathbf{u}(\Omega_2)\big|_{q_1}\right]. \tag{1}$$

$$\mathbf{u}\big|_{q_2} = \frac{1}{2}\left[\mathbf{u}(\Omega_1)\big|_{q_2} + \mathbf{u}(\Omega_3)\big|_{q_2}\right] \tag{2}$$

$$\mathbf{u}\big|_{q_3} = \frac{1}{2}\left[\mathbf{u}(\Omega_1)\big|_{q_3} + \mathbf{u}(\Omega_4)\big|_{q_3}\right] \tag{3}$$

(3) Following the standard FEM procedure for the construction of the quadratic triangular elements [Zienkiewicz and Taylor (2000)], a quadratic displacement field in each of cell is reconstructed using three vertexes of a cell (as the true nodes) and the three midpoints of cell-edge (as the virtual nodes).

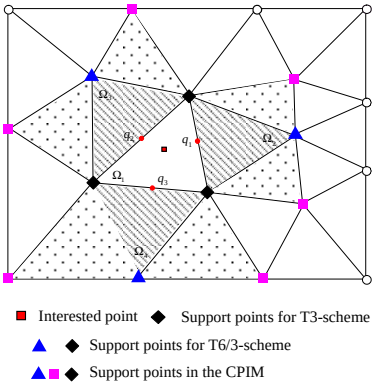

Fig. 1. Influence domain of an interested point in a background cell.

Note that three vertexes of a triangular cell and midpoints of interface edge are respectively same in two adjacent cells. Therefore, when the quadratic interpolation is used, the displacement along interface edge becomes continuous in between two adjacent cells. Hence, we can always obtain a conforming and piecewise quadratic displacement field over the whole problem domain.

The differences between in quadratic FEM and CPIM are: In a quadratic FEM, there are three real nodes at the midpoints of the element edges, and the interpolation operation is performed within each triangular element. In the CPIM, each midpoint on the cell-edges is only a virtual node, and the displacement in a cell is a linear combination of those six sets of the quadratic PIM shape functions involving real nodes beyond the cell in the middle as shown in Fig. 1. As a result, the CPIM selects a total of 12 support nodes for an internal cell shown in Fig. 1 for interpolation [Xu et al. (2010)].

Using the CPIM shape functions, the displacement field can be approximated as follows.

$$\hat{\mathbf{u}}(\mathbf{x}) = \sum_{i \in n_e} \mathbf{\Phi}_i(\mathbf{x})\hat{\mathbf{d}}_i \tag{4}$$

where n_e is the set of nodes in the support domain containing $\mathbf{x}$, $\hat{\mathbf{d}}_i$ is the vector of nodal displacements and

$$\mathbf{\Phi}_i(\mathbf{x}) = \begin{bmatrix} \varphi_i(\mathbf{x}) & 0 \\ 0 & \varphi_i(\mathbf{x}) \end{bmatrix} \tag{5}$$

is the matrix of the CPIM shape functions for node i.

Because the CPIM shape functions are continuous over the problem domain, the compatible strain field can be obtained using

$$\hat{\boldsymbol{\varepsilon}}(\mathbf{x}) = \sum_{i \in n_e} \mathbf{L}_{\mathrm{d}} \left[\boldsymbol{\Phi}_i(\mathbf{x}) \right] \hat{\mathbf{d}}_i \equiv \sum_{i \in n_e} \mathbf{B}_i \hat{\mathbf{d}}_i \tag{6}$$

3 Node-based smoothed CPIM (NS-CPIM)

The present NS-CPIM uses the W^2 formulation with node-based smoothing domains. A node-based smoothed strain is employed in place of compatible strain to construct the system equations. The smoothed strain associated with edge *i* is obtained using the following generalized smoothing operation

$$\bar{\boldsymbol{\varepsilon}} \equiv \frac{1}{A} \int_{\Omega_i} \tilde{\boldsymbol{\varepsilon}}(\mathbf{x}) \mathrm{d}\xi \tag{7}$$

where $\tilde{\boldsymbol{\varepsilon}}(\mathbf{x}) = \mathbf{L}_{\mathbf{d}} \hat{\mathbf{u}}(\mathbf{x})$ is the compatible strain, Ω_i represents the node-based smoothing domain, A is the area of smoothing domain Ω_i.

The node-based smoothing domains are constructed by sequentially connecting the centroids with the mid-edge-points of the surrounding triangles of a node, as illustrated in Fig. 2.

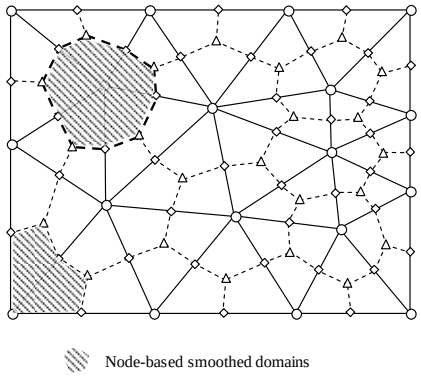

Fig. 2. Triangular background cells and the node-based smoothed domains.

Using the smoothed strain, the “smoothed” energy functional can now be defined as 12]:

$$\hat{\Pi}(\mathbf{v}) = \sum_{i=1}^{N} \left[\frac{1}{2} \int_{\Omega_i} \bar{\boldsymbol{\varepsilon}}^{\mathrm{T}} \mathbf{D} \bar{\boldsymbol{\varepsilon}} \, \mathbf{d}\Omega - \int_{\Omega} \mathbf{v}^{\mathrm{T}} \mathbf{b} \, \mathbf{d}\Omega - \int_{\Gamma_t} \mathbf{v}^{\mathbf{T}} \mathbf{T} \mathrm{d}\Gamma \right] \tag{8}$$

which has exactly the same “form” as the standard Galerkin weak form. Thus, the formulation procedure is quite similar as that in the standard FEM and all we need to do is to use the node-based smoothed strain $\bar{\boldsymbol{\varepsilon}}$ in place of the compatible strain $\tilde{\boldsymbol{\varepsilon}}$.

The overall procedure of the presented methods is as follows. First, the displacement field is constructed by using the CPIM with T6/3 schemes. Then, the

smoothed strains $\bar{\boldsymbol{\varepsilon}}$ are obtained using the method detailed in Section 2 and Section 3. Fnally, by substituting the assumed displacements and the smoothed strains into the generalized Galerkin weak form using functional defined in Eq. (8), a set of discretized algebraic system equations can be obtained in the matrix form

$$\hat{\mathbf{K}}\hat{\mathbf{d}} = \hat{\mathbf{f}}\,, \tag{9}$$

Where

$$\hat{\mathbf{f}} = -\int_{\Omega} \boldsymbol{\Phi}^{\mathrm{T}}\mathbf{b}\mathrm{d}\Omega + \int_{\Gamma_t} \boldsymbol{\Phi}^{\mathrm{T}}\mathbf{T}\mathrm{d}\Gamma\,, \tag{10}$$

and $\hat{\mathbf{K}}$ is the stiffness matrix

$$\hat{K}_{ij} = \sum_{\Omega_e} \hat{k}_{ij} = \sum_{\Omega_e} \int_{\Omega} \mathbf{B}_i^{\mathrm{T}}\mathbf{D}\mathbf{B}_j \mathrm{d}\Omega\,, \tag{11}$$

It has been proven [Liu (2009a)] that the stiffness matrix $\hat{\mathbf{K}}$ obtained from CPIM is *strictly* symmetric positive definite, when the node-based smoothing domains are used.

It is clear from this section that more nodes are participated in construction of shape functions in the present NS-CPIM. Such a "spread" interpolation, together with the softening effects of the smoothing operations, we shall be able to overcome the "overly-stiff" phenomenon of the standard FEM. The effectiveness of these operations will be examined in the following sections.

4. Numerical examples

In this section, a number of numerical examples will be presented to examine the NS-CPIM. To investigate quantitatively the numerical results, the error indicators in displacement norms is defined as follows,

$$E_d = \sqrt{\frac{\sum_{i=1}^{n}\left(\mathbf{u}_i^{ref} - \mathbf{u}_i^{num}\right)^2}{\sum_{i=1}^{n}\left(\mathbf{u}_i^{ref}\right)^2}} \tag{12}$$

where the superscript *ref* denotes the reference or analytical solution, *num* denotes a numerical solution obtained using a numerical method, $\mathbf{u}_i$ denotes the nodal displacement solution, U_{num} is the total strain energy solution, and U_{ref} is the reference or analytical solution of the strain energy.

4.1. *Path test*

For a numerical method working for solid mechanics problems, the sufficient requirement for convergence is to pass the path test [Zienkiewicz and Taylor (2000)]. Therefore, the first example is the standard and quadratic path test using the present NS-CPIM. The following two cases are examined. Case 1 is the standard linear patch test, and case 2 is quadratic patch test.

Case 1: A rectangular patch of 50×10 is considered shown in Fig.3. The displacements are prescribed on all outside boundaries by the following linear function.

$$\begin{cases} u_x = 0.6x \\ u_y = 0.6y \end{cases} \tag{13}$$

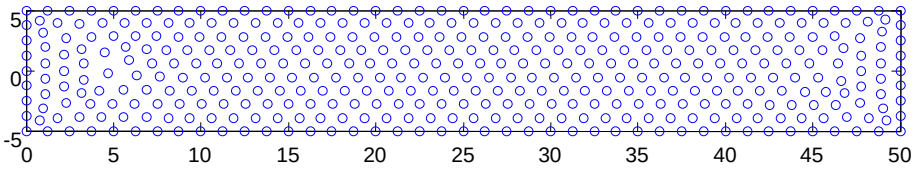

Fig. 3. Node distributions for the standard patch test.

Case 2: A high-order patch of 3×6 (shown in Fig. 4) is considered for patch test. A linearly variable normal stress is applied on the right end. The exact solution for this problem should be

$$u_x = 2xy/3, u_y = -(x^2 + y^2/4)/3 \tag{14}$$

It can be computed that the error E_d obtained using quadratic CPIM are less than 1.0×10^{-14} in case 1 and less than 1.0×10^{-12} in Case 2, which verifies numerically that the NS-CPIM can pass the standard path test and quadratic patch test.

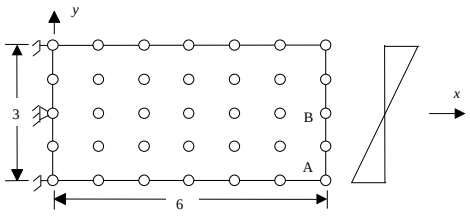

Fig.4 Nodal arrangement for high-order patch test

4.2. *Cantilever 2D beam*

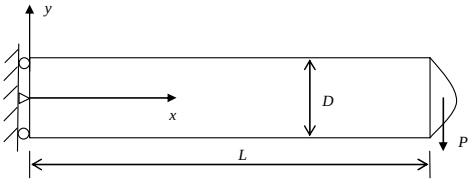

Fig. 5. A 2D cantilever solid subjected to a parabolic traction on the right edge

A 2D cantilever beam with length $L = 50\text{m}$ and height $D = 10\text{m}$ is now studied. The solid is subjected to a parabolic traction at the right end as shown in Fig.5. Analytical solutions can be found in [Timoshenko and Goodier (1970)].

Figure 6 show the convergence status of the strain energies against the increase of DOF for different numerical methods. The exact solution of the strain energy is calculated using the analytical solutions. It can be clearly observed the strain energies of FEM and CPIM always smaller than the exact solution; on the contrary, the strain energies of NS-PIM (T3) and NS-CPIM modes are larger than the exact solution. Furthermore, the NS-CPIM produces an upper bound solution with a higher accuracy than that in NS-PIM (T3). This example shows the very important fact that we now can bound *tightly* the exact solution from both sides using the NS-CPIM and CPIM.

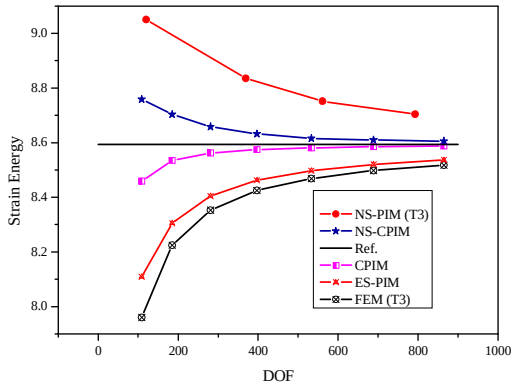

Fig. 6 Solution bounds in energy norm for 2D beam; NS-CPIM produces a "tight" upper bound solution.

4.3. *Infinite 2D solid with a circular hole*

A benchmark problem of an infinite 2D solid with a central circular hole and subjected to a unidirectional tensile is studied (see Fig. 7).

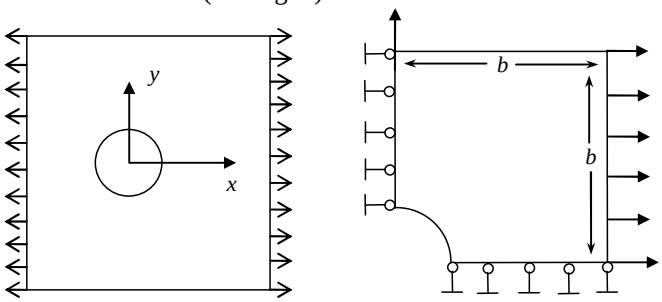

Fig.7. Infinite 2D solid with a hole subjected to a tensile force and its quarter model.

In a similar way to Section 4.2, the strain energies for different methods are computed and plotted in Figure 8. It is clear that NS-CPIM produces a very tight upper

bound solution in strain energy, which indicates that NS-CPIM and CPIM can bound *tightly* the exact solution from both sides.

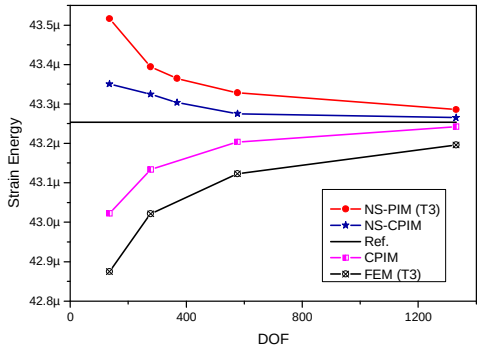

Fig. 8 Strain energy for 2D solid with a circular hole; NS-CPIM produces a "tight" upper bound solution.

Now we consider the problem of nearly incompressible (Poisson's ratio approaching 0.5) in plane strain case using this example. Fig. 9 shows the displacement error norm vs. different Poisson's ratios for the FEM, NS-PIM (T3), CPIM and NS-CPIM. The results show that the FEM, and CPIM are clearly suffered from the volumetric locking. Both NS-PIM (T3) and NS-CPIM can obviously avoid the volumetric locking naturally; while NS-CPIM has the higher accuracy which is recommended for the problem of nearly incompressible by this paper.

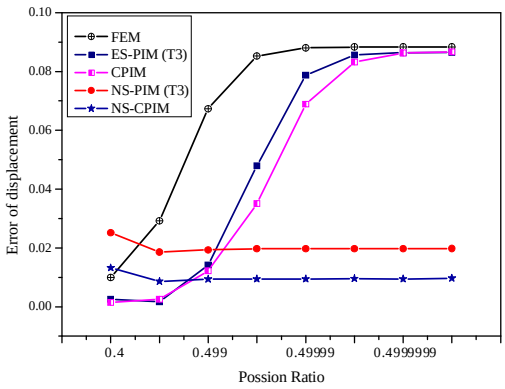

Fig.9. Displacement error norm vs. different Poisson's ratios

4.4. *An L-shaped Component*

An elastic L-shaped component subjected to a pressure load is shown in Fig.10. Plane stress condition is assumed and the reference solution of strain energy is obtained using FEM with a very fine mesh. In a similar way to above Sections, the strain energies for different methods are computed and plotted in Figure 11. It is clear that NS-CPIM

produces a very tight upper bound solution in strain energy, which indicates that NS-CPIM and CPIM can bound *tightly* the exact solution from both sides.

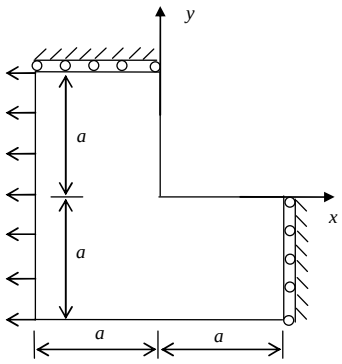

Fig.10. L-shaped plate

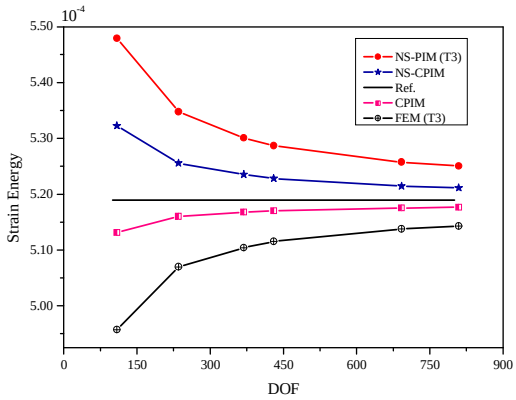

Fig. 11 Convergence in energy norm for L-shaped plate

5. Conclusions

In this work, we proposed a node-based smoothed CPIM (NS-CPIM) by the CPIM shape functions and a W2 formulation. A continuous displacement field in whole problem domain is constructed first; the node-based smoothed strain is then obtained using the strain smoothing technique. By substituting the assumed displacements and the smoothed strains into the generalized smoothed Galerkin weak form, a set of discretized system equations are achieved. The conforming displacement fields and the node-based smoothing operations guarantee the stability and convergence, while ensuring the softening-effect to the system. Theoretical analysis and intensive numerical studies lead to the following conclusions: (1) CPIM can pass both the standard patch test and quadratic patch test; (2) NS-CPIM provides a upper bound of strain energy with very high accuracy for any practical model with a reasonable number of nodes; (3) NS-CPIM

can generally avoid the volumetric locking with a high accuracy, and is recommended for the nearly incompressible problems; (4) NS-CPIM is one of the higher order W2 model, which produces the solutions with high accuracy.

Acknowledgments

This work was supported in part by the Program for New Century Excellent Talents in University (NCET), by the 985 program, by the 211 project of Jilin University, and by Basic funds for science and research in Jilin University. The authors would like to thank the support of A*Star, Singapore, and the Open Research Fund Program of the State Key Laboratory of Advanced Technology of Design and Manufacturing for Vehicle Body, Hunan University, PR.China under Grant no. 40915001. This work is also supported by the NSFC under grant number 11072086.

References

Atluri, S. N. and Zhu, T. (1998). A new meshless local Petrov–Galerkin (MLPG) approach in computational mechanics. *Computational Mechanics*, **22**: 117–127.

Belytschko, Y., Lu, Y. Y. and Gu, L. (1994). Element-free Galerkin methods. *International Journal for Numerical Methods in Engineering*, **37**: 229–256.

Chen, J. S., Wu, C. T., Yoon, S. and You, Y. (2001). A stabilized conforming nodal integration for Galerkin mesh-free methods. *International Journal for Numerical Methods in Engineering* **50**:435–466.

Gu Y.T. (2005), Meshfree methods and their comparisons. *International Journal of Computational Methods*. 2(4), 477-515.

Liu G.R. and Gu Y.T.(2002), Comparisons of two meshfree local point interpolation methods for structural analyses. *Computational Mechanics*, 29(2), 107-121.

Liu G.R. and Gu Y.T.(2001), A point interpolation method for two-dimensional solids. *International Journal for Numerical Methods in Engineering*, 50 (4), 937-951.

Liu, G. R. and Gu, Y. T. (2005). *An Introduction to Meshfree Methods and Their Programming*. Springer: Dordrecht, the Netherlands.

Liu, G. R. (2008). A generalized gradient smoothing technique and the smoothed bilinear form for Galerkin formulation of a wide class of computational methods, *International Journal of Computational Methods*, 5:199–236.

Liu, G. R. and Zhang, G. Y. (2008). Edge-based smoothed point interpolation methods, *International Journal of Computational Methods*, **5**: 621-646.

Liu, G. R. (2009a). Meshfree methods: Moving Beyond the Finite Element Method, 2nd Edition, CRC Press: Boca Raton, USA.

Liu, G. R. (2009b). On a G space theory. *International Journal of Computational Methods*,**6**: 257-289.

Liu, G. R., (2010a). A G space theory and a weakened weak (W2) form for a unified formulation of compatible and incompatible methods: Part I: Theory. Applications to solid mechanics problems, *International Journal for Numerical Methods in Engineering*, **81**: 1093-1126.

Liu, G. R. (2010b) A G space theory and a weakened weak (W2) form for a unified formulation of compatible and incompatible methods: Part II applications to solid mechanics problems. *International Journal for Numerical Methods in Engineering*, **81**: 1127-1156.

Liu, W. K., Jun, S. and Zhang, Y.F. (1995). Reproducing kernel particle methods. *International Journal for Numerical Methods in Engineering*, **20**: 1081–1106.

Timoshenko, S, P. and Goodier, J. N. (1970) *Theory of Elasticity* (3rd edn). McGraw: New York.

Xu, X., Liu, G. R., Gu, Y. T. and Zhang, G. Y. (2010) A conforming point interpolation method (CPIM) by shape function reconstruction for elasticity problems, *International Journal of Computational Methods*, **7**: 369-395.

Zienkiewicz, O. C. and Taylor, R. L. (2000) *The Finite Element Method* (5th edn). Butterworth Heinemann: Oxford, U.K.